https://doi.org/10.15407/ujpe63.9.769

A.V. RUDAKOVSKYI,[1, 2, 3] D.O. SAVCHENKO [1, 3]

[1] Bogolyubov Institute for Theoretical Physics, Nat. Acad. of Sci. of Ukraine
*(14b, Metrolohichna Str., Kyiv 03143, Ukraine; e-mail: rudakovskyi@bitp.kiev.ua)*
[2] Taras Shevchenko National University of Kyiv
*(2, Academician Glushkov Prosp., Kyiv 03022, Ukraine)*
[3] Main Astronomical Observatory, Nat. Acad. of Sci. of Ukraine
*(27, Academician Zabolotnyi Str., Kyiv 03143, Ukraine)*

# NEW MODEL OF DENSITY DISTRIBUTION FOR FERMIONIC DARK MATTER HALOS

*We formulate a new model of density distribution for halos made of warm dark matter (WDM) particles. The model is described by a single microphysical parameter – the mass (or, equivalently, the maximal value of the initial phase-space density distribution) of dark matter particles. Given the WDM particle mass and the parameters of a dark matter density profile at the halo periphery, this model predicts the inner density profile. In the case of initial Fermi–Dirac distribution, we successfully reproduce cored dark matter profiles from N-body simulations. We calculate also the core radii of warm dark matter halos of dwarf spheroidal galaxies for particle masses* $m_{\rm FD} = 100$, 200, 300, *and* 400 *eV.*

*K e y w o r d s*: dark matter: warm, cold; dark matter halo profile; cores; Navarro–Frenk–White profile.

## 1. Introduction

The nature of dark matter – the largest gravitating substance in the Universe – is not yet identified. Usual (left-handed) neutrinos – the only natural dark matter candidate within the Standard Model of particle physics – are too light to form the observed large-scale structure of the Universe [1] and the densest dark matter-dominated objects, dwarf spheroidals (dSphs) [2]. So far, many extensions of the Standard Model containing a viable dark matter candidate have been proposed; see, e.g., reviews [3–6]. In terms of their initial velocities, valid dark matter candidates can be split in two groups [1] (see, e.g., [9]):

• cold dark matter (CDM) composed of particles with small (non-relativistic) initial velocities [10, 11];

• warm dark matter (WDM) composed of particles with large (relativistic) initial velocities [12, 13].

The density distribution of CDM haloes is often described by the Navarro–Frenk–White (NFW) profile [14, 15]

$$\rho_{\rm NFW}(r) = \frac{\rho_s r_s}{r\left(1+\frac{r}{r_s}\right)^2}. \qquad (1)$$

Its parameters $\rho_s$ and $r_s$ are connected with the halo mass $M_{200}$ (the mass within the sphere of radius $R_{200}$, within which the average density is 200 times larger than the critical density $\rho_{\rm crit}$ of the Universe) and halo concentration parameter $c_{200} = R_{200}/r_s$.

[1] Note that, for some specific dark matter particle candidates, their initial velocity spectrum can be approximated by a mixture of "cold" and "warm" components [7, 8].

The phase-space density for CDM haloes becomes *infinite* toward the halo center; see, e.g., [16]. For WDM, this is not true: its maximal phase-space density $f_{\max}$ is finite at early times and does not increase during the halo formation [17]. Usually, the density distributions with finite $f_{\max}$ are derived either from analytical studies of self-gravitating Fermi–Dirac dark matter (see, e.g., [18–27]) or from $N$-body simulations imitating initial dark matter velocities (see, e.g., [28–32]).

The first method requires non-trivial assumptions about dark matter microphysics. In addition, it often has problems with a *simultaneous* description of the whole dark matter halo including the central part (where the dark matter phase-space density is close to $f_{\max}$) and the outskirts (where it is $\ll f_{\max}$). This, in turn, is well-established by $N$-body simulations. But simulations are computationally expensive; to determine the dark matter properties, one requires too many of them to compare to specific observations.

In this paper, we present a new model of density distribution that overcomes both difficulties. It is constructed in Sec. 2 avoiding any assumptions about dark matter microphysics apart from the knowledge of the maximal value of the dark matter phase-space density. As we show in Sec. 3 3.1, this model predicts the flattening of the inner density profile at small radii (producing dark matter *cores*) consistent with WDM simulations [28, 29]. In Sec. 3 3.2, we study the formation of dark matter cores for 'classical' and "ultra-faint" dSphs [2]. Finally, in Sec. 4, we discuss the obtained results.

## 2. Method

According to strong Jeans' theorem [34–36], the phase-space density distribution $f(\mathbf{r}, \mathbf{v})$ of a collisionless system in the steady state depends on coordinates $\mathbf{r}$ and velocities $\mathbf{v}$ only through the isolating [37] integrals of motion. Assuming the steady-state dark matter halo to be non-rotating, isotropic, and spherically symmetric [3], the phase-space density $f(\mathbf{r}, \mathbf{v})$ of dark matter particles with mass $m_{\rm FD}$ inside the halo depends *only* on their total energy $\mathcal{E}$, $E \equiv \frac{\mathcal{E}}{m_{\rm FD}} = v^2/2 + \Phi(r)$ [36], where $\Phi(r)$ is the local gravitational potential:

$$\Phi(r) = -4\pi G_N \int\limits_r^\infty \frac{dx}{x^2} \int\limits_0^x \rho(y) y^2 dy. \tag{2}$$

Under this assumption, the Eddington transformation [36, 66, 67] unambiguously determines the phase-space density distribution given the dark matter density $\rho$:

$$f(E) = \frac{1}{\pi^2\sqrt{8}} \frac{d}{dE} \int\limits_E^0 \frac{d\rho}{d\Phi} \frac{d\Phi}{\sqrt{E-\Phi}}. \tag{3}$$

We start from dark matter haloes with the NFW dark matter density distribution; see Eq. (1). For such haloes, the phase-space density $f_{\rm NFW}(E)$ becomes infinite as $E \to \Phi(0) \equiv -4\pi G_N \rho_s r_s^2$ [68]. This behavior contradicts the expectations of the WDM model: according to the Liouville theorem, $f(E)$ should not exceed some finite maximal value $f_{\max}$ of the initial phase-space density defined by dark matter microphysics. A particular example of interest is dark matter with the initial Fermi–Dirac distribution having particle mass $m_{\rm FD}$ and $g$ internal degrees of freedom. For this dark matter model, the maximal value of the initial phase-space density is [17]

$$f_{\max} = \frac{g m_{\rm FD}^4}{2(2\pi\hbar)^3} = \\ = 1.31 \times 10^4 \left(\frac{g}{2}\right) \left(\frac{m_{\rm FD}}{400\ \text{eV}}\right)^4 \ M_\odot/\text{kpc}^3(\text{km/s})^3 \tag{4}$$

(henceforth, we assume $g = 2$). For any other dark matter particle model with known $f_{\max}$, one can express it in terms of $m_{\rm FD}$, by using Eq. (4).

[2] For the dSphs nomenclature, see, e.g., [33, Sec. 1.1].

[3] For the observed dSphs, some of these assumptions can be violated. For example, Sagitarrius [38, 39], Ursa Major II [40, 41], and Boötes III [42] dSphs are reported to be tidally disrupted, which puts the assumption of steady state in these objects under question. Based on works [43–51], we expect only slight deviations from the velocity isotropy in the central parts of dark matter haloes. Although the authors of [52, 53] reported on deviations from the spherical symmetry in dark matter haloes of dSphs, it is unclear to what extent their result can affect the density distribution. For example, according to [54], the absence of spherical symmetry does not change the conclusion of [55] about the presence of dark matter cores in dSphs (see, however, [56]). Moreover, it was shown in [57] that smaller galaxies tend to be more spherically symmetric, and the dark matter distribution is more spherically symmetric than the stellar distribution. Finally, although rotations are detected in several individual objects (see, e.g., [40, 58–60]), spectroscopic observations [61–65] showed the absence of rotations with velocities comparable with the observed velocity dispersions in dSphs.

To account for the maximal phase-space density, we *truncate* $f(E)$ in a way that it cannot exceed the pre-selected maximal value $f_{\max}$:

$$f_{\rm tNFW}(E) = \begin{cases} f_{\rm NFW}(E), & f_{\rm NFW}(E) < f_{\max}, \\ f_{\max}, & f_{\rm NFW}(E) \geq f_{\max}. \end{cases} \quad (5)$$

The obtained phase-space density $f_{\rm tNFW}(E)$ is then converted to the mass density via [67]

$$\rho_{\rm tNFW}(r) = 4\pi \int\limits_{\Phi(r)}^{0} f_{\rm tNFW}(E)\sqrt{2\left(E-\Phi(r)\right)}dE. \quad (6)$$

Since the potential $\Phi(r)$ in Eq. (6) depends on the actual $\rho(r)$, we can solve the system of equations (3)–(6) *iteratively*. We use the following iterative procedure: we calculate numerically the $\Phi_{i-1}(r)$ and $f_{i-1}(E)$ from the density distribution $\rho_{i-1}(r)$ obtained in the previous step. Then we truncate $f_{i-1}(E)$ as in Eq. (3) and obtain the new density distribution $\rho_i(r)$ from this truncated distribution function, by using Eq. (6). We perform all the calculations on a grid in the interval $(r_0, r_{\max})$. We choose $r_0 \ll r_s$ for the regularization at the first iteration. The quantity $r_{\max}$ is defined as $\rho_{\rm NFW}(r_{\max}) = \bar{\rho}_{\rm DM}$, and $r_{\max} \gg R_{200}$, so we use it as the upper limit of integration in Eq. (2). We use the value $\max\left|\frac{\rho_i(r)-\rho_{i-1}(r)}{\rho_{i-1}(r)}\right|$ as a convergence criterion. As demonstrated in Fig. 1, five iterations are sufficient to achieve the convergence for our chosen grid parameters ($\max\left|\frac{\rho_5(r)-\rho_4(r)}{\rho_4(r)}\right| < 0.01$). We demonstrate the convergence of this iterative procedure by the numerous numerical tests and do not strictly prove it. The obtained results show the very weak dependence of the obtained truncated density profiles on the grid parameters.

## 3. Results

### 3.1. Comparison with N-body simulations

To check the validity of the proposed approach, we compared the truncated dark matter density distribution $\rho_{\rm tNFW}(r)$ to the results of two independent $N$-body simulations [28,29]. Both simulations include the effect of maximal phase-space density by assigning non-zero initial velocities to dark matter particles. More precisely, [28] assumes the Fermi–Dirac distribution $f(v) = [\exp(v/v_0)+1]^{-1}$, where $v_0$ is the characteristic velocity of dark matter particles [69], while [29] approximates it with a *Gaussian* velocity distribution.

In Figure, we compare the tNFW density profile to simulation P-WDM$_{512}$ from [28] and simulation WDM-5 from [29], corresponding to $m_{\rm FD} = 30$ eV and 23 eV, respectively [4]. We extracted the NFW parameters from Fig. 2 of [28] and Fig. 2 of [29], respectively, and calculated the corresponding tNFW profiles. Figure shows that the tNFW profiles match the corresponding WDM distributions at the $\lesssim$30% level. We do not observe any systematic disagreement between the tNFW profile and other WDM profiles from $N$-body simulations [28, 29, 31].

### 3.2. Core radii of dwarf spheroidal galaxies

An important property of the distribution $\rho_{\rm tNFW}(r)$ is its flattening toward small radii. This flattening is usually characterized by the radius of the so-called *dark matter core* [5]. In this paper, we define the core radius $r_c$ for a given dark matter distribution $\rho_{\rm DM}(r)$ as follows:

$$\rho_{\rm tNFW}(r_c) = \frac{\rho_{\rm tNFW}(0)}{4}. \quad (7)$$

This definition coincides with the characteristic radius of the widely used Burkert density distribution [71], as well as with the core radius defined in [24, 72]. The largest effect from a finite phase-space density on the core sizes is expected in the systems hosted by the densest dark matter haloes – dwarf spheroidals (dSphs).

We analyzed the two types of halos of dwarf spheroidals: "classical" dSph with corresponding NFW parameters $M_{200} = 4\times10^8$ M$_\odot$ and $c_{200} = 30$, and "ultra-faint" dSph with $M_{200} = 1\times10^8$ M$_\odot$ and

[4] The last number differs from the value reported in Table 1 of [29] To obtain it, we took into account that [29] assumed the Gaussian velocity distribution with the velocity dispersion $\sigma = 3.571 v_0$ [69], so that their maximal phase-space density can be calculated from the dark matter density $\rho_{\rm DM}$:

$$f_{\max} = \frac{\rho_{\rm DM}}{(2\pi\sigma^2)^{3/2}}.$$

For WDM-5 simulation of [29],

$$f_{\max} = 0.151\ M_\odot\ {\rm kpc}^3({\rm km/s})^3,$$

which corresponds to $m_{\rm FD} = 23$ eV according to Eq. (4).

[5] There are many different definitions of core radii in the literature; see, e.g., [29, 70].

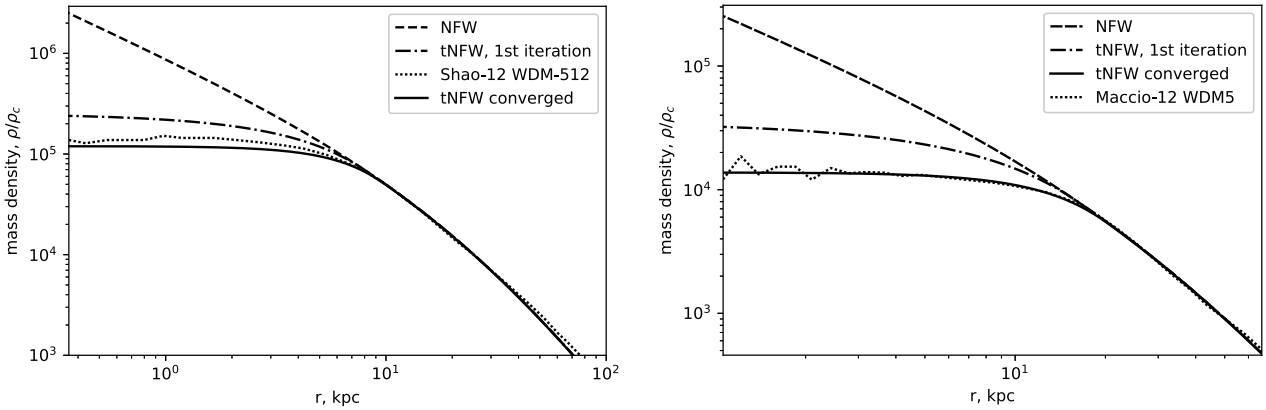


*Left*: Comparison of the tNFW profile with $N$-body simulation P-WDM$_{512}$ of [28]. We started from the NFW profile with $\rho_s = 4.9 \times 10^7$ M$_\odot$/kpc$^3$ and $r_s = 26$ kpc corresponding to the parameters of P-WDM$_{512}$ halo in Fig. 2 of [28]. Then we built the tNFW profile with $m_{\rm FD} = 30$ eV, by using Eqs. (3)–(6). For individual iterations, the mass density profiles (shown by black dash-dotted curve) started to converge quickly, so we used the sixth iteration (shown by a solid curve) as a final tNFW profile. Due to the truncation of the phase-space density distribution, the final value of $M_{200}$ for this tNFW profile becomes $1.27 \times 10^{12}$ M$_\odot$, by decreasing from its initial value by 9%. Note the similarity between the tNFW profile and the result of $N$-body simulations of [28] (dotted curve): the resulting mass densities and core radii differ by less than 30%. *Right*: comparison of the density distribution from simulation WDM-5 of [29] and the corresponding tNFW profile starting from $\rho_s = 1.2 \times 10^6$ M$_\odot$/kpc$^3$, $r_s = 33$ kpc and using $m_{\rm FD} = 23$ eV (see the text). For this tNFW profile, the final value of $M_{200}$ is $4.7 \times 10^{11}$ M$_\odot$, by decreasing from the initial value by 11%. The differences between the density profiles and derived core radii are also $\lesssim$30% in this case

$c_{200} = 40$. Assuming the initial Fermi–Dirac distribution of warm dark matter particles, we generated tNFW profiles with $m_{\rm FD} = 100$, 200, 300, and 400 eV for these halos. The obtained core radii $r_c$ are summarized in Table.

## 4. Discussion

Here, we describe a new simple model to quantify the effect of the maximal phase-space density ($f_{\rm max}$) on the dark matter distribution. In contrast to other models, we start from the well-known Navarro–Frenk–White (NFW) density profile [14, 15] consistent with $N$-body simulations with $f_{\rm max} = \infty$. After that, we truncate the corresponding phase-space density profile at the value of $f_{\rm max}$ and recalculate the corresponding density profile, by using the Eddington transformation [66]. The obtained "truncated NFW" (tNFW) density distribution flattens at small radii, by producing a *core*. Despite its simplicity, the tNFW profile matches the detailed $N$-body simulations from [28,29] with high precision, $\lesssim$30% as demonstrated in Figure.

**Core radii for tNFW density profiles of "classical" and "ultra-faint" dwarf spheroidal galaxies for $m_{\rm FD} = 100$, 200, 300, and 400 eV**

| dSph | $m_{\rm FD}$, eV | $r_c$, kpc |
|---|---|---|
| "classical" | 100 | 3.82 |
| | 200 | 0.86 |
| | 300 | 0.41 |
| | 400 | 0.26 |
| "ultra-faint" | 100 | 5.57 |
| | 200 | 1.08 |
| | 300 | 0.46 |
| | 400 | 0.27 |

The recent papers [24,72] have questioned the lower bound on $m_{\rm FD} \gtrsim 0.48$ keV obtained in [17]. By assuming an anisotropic velocity distribution, the authors of [24] claimed that the velocity dispersion profiles in "classical" dSphs are consistent with the mass of degenerate fermions as low as $m = 0.2$ keV (equivalent to $m_{\rm FD} = 0.24$ keV). Work [72] extended this result, by using data on both "classical" and "ultra-faint" dSphs. According to [72], the lower bound of [17] should be further weakened down to $m_{\rm FD} \gtrsim 0.12$ keV in the case of arbitrary stellar velocity anisotropy and no relation between the stellar and dark matter velocity dispersions.

It was suggested in [73] that the Fornax dSph has a core with $r_c = 1^{+0.8}_{-0.4}$ kpc. To create sizeable cores in

the halos of dwarf galaxies without involving baryonic processes, one requires rather light dark matter particles ($m_{\rm FD} < 300$ eV; see Table). Such dark matter is in tension with a number of constraints from observations of the large-scale structure; see, e.g., recent works [74–85]. However, due to the smallness of their potential wells, the dwarf galaxies are very sensitive to baryonic feedback processes; see, e.g., [86–95]. Working together with the finite dark matter phase-space density effect, these processes could produce much larger cores, with core sizes being close to ∼1 kpc.

*The authors are grateful to D. Iakubovskyi and Yu. Shtanov for the collaboration and valuable comments. This work was partially supported by the National Academy of Sciences of Ukraine (project No. 0116U003191), by the Program of Fundamental Research of the Division of Physics and Astronomy of the National Academy of Sciences of Ukraine (project No. 0117U000240), by grant 6F of the Department of Targeted Training of the Taras Shevchenko National University of Kyiv under the National Academy of Sciences of Ukraine, and by the Program of Cosmic Research of the National Academy of Sciences of Ukraine.*

1. S.D.M. White, C.S. Frenk, M. Davis. Clustering in a neutrino-dominated universe. *Astrophys. J.* **274**, L1 (1983).
2. S. Tremaine, J. E. Gunn. Dynamical role of light neutral leptons in cosmology. *Phys. Rev. Lett.* **42**, 407 (1979).
3. L. Bergström. Non-baryonic dark matter: observational evidence and detection methods. *Rep. Progr. Phys.* **63**, 793 (2000).
4. G. Bertone, D. Hooper, J. Silk. Particle dark matter: Evidence, candidates and constraints. *Phys. Rep.* **405**, 279 (2005).
5. J.L. Feng. Dark matter candidates from particle physics and methods of detection. *Ann. Rev. Astron. Astrophys* **48**, 495 (2010).
6. S. Gardner, G.M. Fuller. Dark matter studies entrain nuclear physics. *Progr. Part. Nucl. Phys.* **71**, 167 (2013).
7. A. Palazzo, D. Cumberbatch, A. Slosar, J. Silk. Sterile neutrinos as subdominant warm dark matter. *Phys. Rev. D* **76**, 10, 103511 (2007).
8. A. Boyarsky, O. Ruchayskiy, M. Shaposhnikov. The role of sterile neutrinos in cosmology and astrophysics. *Ann. Rev. Nucl. Part. Sci.* **59**, 191 (2009).
9. J.R. Primack. Dark matter and structure formation in the universe. arXiv:astro-ph/9707285.
10. S.D. M. White, M.J. Rees. Core condensation in heavy halos – A two-stage theory for galaxy formation and clustering. *Mon. Not. R. Astron. Soc.* **183**, 341 (1978).
11. G.R. Blumenthal, S.M. Faber, J.R. Primack, M.J. Rees. Formation of galaxies and large-scale structure with cold dark matter. *Nature* **311**, 517 (1984).
12. G.S. Bisnovatyi-Kogan, I.D. Novikov. Cosmology with a nonzero neutrino rest mass. *Soviet Ast.* **24**, 516 (1980).
13. J.R. Bond, G. Efstathiou, J. Silk. Massive neutrinos and the large-scale structure of the universe. *Phys. Rev. Lett.* **45**, 1980 (1980).
14. J.F. Navarro, C.S. Frenk, S.D.M. White. The structure of cold dark matter halos. *Astrophys. J.* **462**, 563 (1996).
15. J.F. Navarro, C.S. Frenk, S.D.M. White. A universal density profile from hierarchical clustering. *Astrophys. J.* **490**, 493 (1997).
16. J.E. Taylor, J.F. Navarro. The phase-space density profiles of cold dark matter halos. *Astrophys. J.* **563**, 483 (2001).
17. A. Boyarsky, O. Ruchayskiy, D. Iakubovskyi. A lower bound on the mass of dark matter particles. *J. Cosmol. Astropart. Phys.* **3**, 005 (2009).
18. R. Ruffini, L. Stella. On semi-degenerate equilibrium configurations of a collisionless self-gravitating Fermi gas. *Astron. Astrophys.* **119**, 35 (1983).
19. N. Bilić, R.D. Viollier. Gravitational phase transition of fermionic matter. *Phys. Lett. B* **408**, 75 (1997).
20. G.W. Angus. A lower limit on the dark particle mass from dSphs. *J. Cosmol. Astropart. Phys.* **3**, 026 (2010).
21. H. J. de Vega, P. Salucci, N.G. Sanchez. Observational rotation curves and density profiles versus the Thomas–Fermi galaxy structure theory. *Mon. Not. R. Astron. Soc.* **442**, 2717 (2014).
22. H.J. de Vega, N.G. Sanchez. The dark matter distribution function and halo thermalization from the Eddington equation in galaxies. *Int. J. Mod. Phys. A* **31**, 1650073 (2016).
23. M. Merafina, G. Alberti. Self-gravitating Newtonian models of fermions with anisotropy and cutoff energy in their distribution function. *Phys. Rev. D* **89** (12), 123010 (2014).
24. V. Domcke, A. Urbano. Dwarf spheroidal galaxies as degenerate gas of free fermions. *J. Cosmol. Astropart. Phys.* **1**, 002 (2015).
25. R. Ruffini, C.R. Argüelles, J.A. Rueda. On the core-halo distribution of dark matter in galaxies. *Mon. Not. R. Astron. Soc.* **451**, 622 (2015).
26. P.-H. Chavanis, M. Lemou, F. Méhats. Models of dark matter halos based on statistical mechanics: The fermionic King model. *Phys. Rev. D* **92**, 12, 123527 (2015).
27. C.R. Argüelles, A. Krut, J.A. Rueda, R. Ruffini. Novel constraints on fermionic dark matter from galactic observables. arXiv:1606.07040 [astro-ph.GA].
28. S. Shao, L. Gao, T. Theuns, C.S. Frenk. The phasespace density of fermionic dark matter haloes. *Mon. Not. R. Astron. Soc.* **430**, 2346 (2013).
29. A.V. Macciò, S. Paduroiu, D. Anderhalden, A. Schneider, B. Moore. Cores in warm dark matter haloes: a Catch 22 problem. *Mon. Not. R. Astron. Soc.* **424**, 1105 (2012).
30. A.V. Macciò, S. Paduroiu, D. Anderhalden, A. Schneider, B. Moore. Erratum: Cores in warm dark matter haloes: a

Catch 22 problem. *Mon. Not. R. Astron. Soc.* **428**, 3715 (2013).
31. A. V. Macciò, O. Ruchayskiy, A. Boyarsky, J.C. Muñoz-Cuartas. The inner structure of haloes in cold + warm dark matter models. *Mon. Not. R. Astron. Soc.* **428**, 882 (2013).
32. D. Anderhalden, A. Schneider, A.V. Macciò, J. Diemand, G. Bertone. Hints on the nature of dark matter from the properties of Milky Way satellites. *J. Cosmol. Astropart. Phys.* **3**, 014 (2013).
33. J.S. Bullock, M. Boylan-Kolchin. Small-Scale Challenges to the ΛCDM Paradigm, *Ann. Rev. Astron. Astrophys* **55**, 343 (2017).
34. J.H. Jeans. On the theory of star-streaming and the structure of the universe. *Mon. Not. R. Astron. Soc.* **76**, 70 (1915).
35. D. Lynden-Bell. Stellar dynamics. Only isolating integrals should be used in Jeans theorem. *Mon. Not. R. Astron. Soc.* **124**, 1 (1962).
36. C. Efthymiopoulos, N. Voglis, C. Kalapotharakos. *Special features of galactic dynamics, in Lecture Notes in Physics* edited by D. Benest, C. Froeschle, and E. Lega (Springer, 2007).
37. G. Contopoulos. A classification of the integrals of motion. *Astrophys. J.* **138**, 1297 (1963).
38. R.A. Ibata, G. Gilmore, M.J. Irwin. A dwarf satellite galaxy in Sagittarius. *Nature* **370**, 194 (1994).
39. S.R. Majewski, M.F. Skrutskie, M.D. Weinberg, J.C. Ostheimer. A two micron all sky survey view of the sagittarius dwarf galaxy. I. Morphology of the sagittarius core and tidal arms. *Astrophys. J.* **599**, 1082 (2003).
40. J.D. Simon, M. Geha. The kinematics of the ultrafaint Milky Way satellites: Solving the missing satellite problem. *Astrophys. J.* **670**, 313 (2007).
41. R. Smith, M. Fellhauer, G.N. Candlish, R. Wojtak, J.P. Farias, M. Blaña. Ursa Major II – reproducing the observed properties through tidal disruption. *Mon. Not. R. Astron. Soc.* **433**, 2529 (2013).
42. J.L. Carlin, C.J. Grillmair, R.R. Muñoz, D.L. Nidever, S.R. Majewski. Kinematics and metallicities in the Boötes III stellar overdensity: A disrupted dwarf galaxy? *Astrophys. J.* **702**, L9 (2009).
43. S. Kazantzidis, J. Magorrian, B. Moore. Generating equilibrium dark matter halos: Inadequacies of the local Maxwellian approximation. *Astrophys. J.* **601**, 37 (2004).
44. S.H. Hansen, J. Stadel. The velocity anisotropy – density slope relation. *J. Cosmol. Astropart. Phys.* **5**, 014 (2006).
45. A. Zait, Y. Hoffman, I. Shlosman. Dark matter halos: Velocity anisotropy-density slope relation. *Astrophys. J.* **682**, 835 (2008).
46. M. Sparre, S.H. Hansen. The behavior of shape and velocity anisotropy in dark matter haloes. *J. Cosmol. Astropart. Phys.* **10**, 049 (2012).
47. G.A. Mamon, A. Biviano, G. Boué. MAMPOSSt: Modelling anisotropy and mass profiles of observed spherical systems – I. Gaussian 3D velocities. *Mon. Not. R. Astron. Soc.* **429**, 3079 (2013).
48. L. Beraldo e Silva, G.A. Mamon, M. Duarte, R. Wojtak, S. Peirani, G. Boué. Anisotropic q-Gaussian 3D velocity distributions in ΛCDM haloes. *Mon. Not. R. Astron. Soc.* **452**, 944 (2015).
49. C.A. Vera-Ciro, L.V. Sales, A. Helmi, J.F. Navarro. The shape of dark matter subhaloes in the Aquarius simulations. *Mon. Not. R. Astron. Soc.* **439**, 2863 (2014).
50. K. El-Badry, A.R. Wetzel, M. Geha, E. Quataert, P.F. Hopkins, D. Kereš, T.K. Chan, C.-A. Faucher-Giguère. When the jeans do not fit: How stellar feedback drives stellar kinematics and complicates dynamical modeling in low-mass galaxies. *Astrophys. J.* **835**, 193 (2017).
51. A. Eilersen, S. H. Hansen, X. Zhang. Analytical derivation of the radial distribution function in spherical dark matter haloes. *Mon. Not. R. Astron. Soc.* **467**, 2061 (2017).
52. K. Hayashi, M. Chiba. Probing non-spherical dark halos in the galactic dwarf galaxies. *Astrophys. J.* **755**, 145 (2012).
53. K. Hayashi, M. Chiba. Structural properties of nonspherical dark halos in Milky Way and Andromeda dwarf spheroidal galaxies. *Astrophys. J.* **810**, 22 (2015).
54. C.F.P. Laporte, M.G. Walker, J. Peñarrubia. Measuring the slopes of mass profiles for dwarf spheroidals in triaxial cold dark matter potentials. *Mon. Not. R. Astron. Soc.* **433**, L54 (2013).
55. M.G. Walker, J. Peñarrubia. A method for measuring (slopes of) the mass profiles of dwarf spheroidal galaxies. *Astrophys. J.* **742**, 20 (2011).
56. A. Genina, A. Benítez-Llambay, C.S. Frenk, S. Cole, A. Fattahi, J.F. Navarro, K.A. Oman, T. Sawala, T. Theuns. The core-cusp problem: A matter of perspective. *Mon. Not. R. Astron. Soc.* **474**, 1398 (2018).
57. D.J.R. Campbell, C.S. Frenk, A. Jenkins, V.R. Eke, J.F. Navarro, T. Sawala, M. Schaller, A. Fattahi, K.A. Oman, T. Theuns. Knowing the unknowns: Uncertainties in simple estimators of galactic dynamical masses. *Mon. Not. R. Astron. Soc.* **469**, 2335 (2017).
58. N.C. Amorisco, N. W. Evans. A troublesome past: Chemodynamics of the fornax dwarf spheroidal. *Astrophys. J.* **756**, L2 (2012).
59. N. Ho, M. Geha, R.R. Muñoz, P. Guhathakurta, J. Kalirai, K.M. Gilbert, E. Tollerud, J. Bullock, R.L. Beaton, S.R. Majewski. Stellar kinematics of the Andromeda II dwarf spheroidal galaxy. *Astrophys. J.* **758**, 124 (2012).
60. A. del Pino, E.L. Łokas, S.L. Hidalgo, S. Fouquet. The structure of Andromeda II dwarf spheroidal galaxy. *Mon. Not. R. Astron. Soc.* **469**, 4999 (2017).
61. M.G. Walker, M. Mateo, E.W. Olszewski, R. Bernstein, X. Wang, M. Woodroofe. Internal kinematics of the Fornax dwarf spheroidal galaxy. *AJ* **131**, 2114 (2006).
62. A. Koch, M.I. Wilkinson, J.T. Kleyna, G.F. Gilmore, E.K. Grebel, A.D. Mackey, N.W. Evans, R.F.G. Wyse. Stellar kinematics and metallicities in the Leo I dwarf spheroidal galaxy-wide-field implications for galactic evolution. *Astrophys. J.* **657**, 241 (2007).

63. P.M. Frinchaboy, S.R. Majewski, R.R. Muñoz, D.R. Law, E.L. Lokas, W.E. Kunkel, R.J. Patterson, K.V. Johnston. A 2MASS All-sky view of the Sagittarius Dwarf Galaxy. VII. Kinematics of the main body of the Sagittarius dSph. *Astrophys. J.* **756**, 74 (2012).
64. A.W. McConnachie. The Observed Properties of Dwarf Galaxies in and around the Local Group. *Astron. J.* **144**, 4 (2012).
65. M.E. Spencer, M. Mateo, M.G. Walker, E.W. Olszewski. A multi-epoch kinematic study of the remote dwarf spheroidal galaxy Leo II. *Astrophys. J.* **836**, 202 (2017).
66. A.S. Eddington. The distribution of stars in globular clusters. *Mon. Not. R. Astron. Soc.* **76**, 572 (1916)
67. J. Binney, S. Tremaine. *Galactic Dynamics* (Princeton Univ. Press, 2008).
68. L.M. Widrow. Distribution functions for cuspy dark matter density profiles. *Astrophys. J. Suppl.* **131**, 39 (2000).
69. P. Bode, J.P. Ostriker, N. Turok. Halo formation in warm dark matter models. *Astrophys. J.* **556**, 93 (2001).
70. L. Randall, J. Scholtz, J. Unwin. Cores in dwarf Galaxies from Fermi repulsion. *Mon. Not. R. Astron. Soc.* **467**, 1515 (2017).
71. A. Burkert. The structure of dark matter halos in dwarf galaxies. *Astrophys. J.* **447**, L25 (1995).
72. C. Di Paolo, F. Nesti, F.L. Villante. Phase-space mass bound for fermionic dark matter from dwarf spheroidal galaxies. *Mon. Not. R. Astron. Soc.* **475**, 5385 (2018).
73. N.C. Amorisco, A. Agnello, N.W. Evans. The core size of the Fornax dwarf spheroidal. *Mon. Not. R. Astron. Soc.* **429**, L89 (2013).
74. J.I. Read, G. Iorio, O. Agertz, F. Fraternali. The stellar mass-halo mass relation of isolated field dwarfs: a critical test of ΛCDM at the edge of galaxy formation. *Mon. Not. R. Astron. Soc.* **467**, 2019 (2017).
75. P.S. Corasaniti, S. Agarwal, D.J.E. Marsh, S. Das. Constraints on dark matter scenarios from measurements of the galaxy luminosity function at high redshifts. *Phys. Rev. D* **95** (8), 083512 (2017).
76. A. Schneider, S. Trujillo-Gomez, E. Papastergis, D.S. Reed, G. Lake. Hints against the cold and collisionless nature of dark matter from the galaxy velocity function. *Mon. Not. R. Astron. Soc.* **470**, 1542 (2017).
77. N. Menci, A. Merle, M. Totzauer, A. Schneider, A. Grazian, M. Castellano, N.G. Sanchez. Fundamental physics with the hubble frontier fields: Constraining dark matter models with the abundance of extremely faint and distant galaxies. *Astrophys. J.* **836**, 61 (2017).
78. J.F. Cherry, S. Horiuchi. Closing in on resonantly produced sterile neutrino dark matter. *Phys. Rev. D* **95** (8), 083015 (2017).
79. S. Birrer, A. Amara, A. Refregier. Lensing substructure quantification in RXJ1131-1231: A 2 keV lower bound on dark matter thermal relic mass. *J. Cosmol. Astropart. Phys.* **5**, 037 (2017).
80. V. Iršič, M. Viel, M.G. Haehnelt, J.S. Bolton, S. Cristiani, G.D. Becker, V. D'Odorico, G. Cupani, T.-S. Kim, T.A.M. Berg, S. López, S. Ellison, L. Christensen, K.D. Denney, G. Worseck. New constraints on the free-streaming of warm dark matter from intermediate and small scale Lyman-$\alpha$ forest data. *Phys. Rev. D* **96** (2), 023522 (2017).
81. C. Yèche, N. Palanque-Delabrouille, J. Baur, H. du Mas des Bourboux. Constraints on neutrino masses from Lyman-alpha forest power spectrum with BOSS and XQ-100. *J. Cosmol. Astropart. Phys.* **6**, 047 (2017).
82. L. Lopez-Honorez, O. Mena, S. Palomares-Ruiz, P. Villanueva-Domingo. Warm dark matter and the ionization history of the Universe. *Phys. Rev. D* **96** (10), 103539 (2017).
83. P. Dayal, T.R. Choudhury, F. Pacucci, V. Bromm. Warm dark matter constraints from high-z direct collapse black holes using the JWST. *Mon. Not. R. Astron. Soc.* **472**, 4414 (2017).
84. J. Baur, N. Palanque-Delabrouille, C. Yèche, A. Boyarsky, O. Ruchayskiy, É. Armengaud, J. Lesgourgues. Constraints from Ly-$\alpha$ forests on non-thermal dark matter including resonantly-produced sterile neutrinos. *J. Cosmol. Astropart. Phys.* **12**, 013 (2017).
85. N. Menci, E. Giallongo, A. Grazian, D. Paris, A. Fontana, L. Pentericci. Observing the very low surface brightness dwarfs in a deep field in the VIRGO cluster: Constraints on dark matter scenarios. *Astron. Astrophys.* **604**, A59 (2017).
86. A. Dekel, J. Silk. The origin of dwarf galaxies, cold dark matter, and biased galaxy formation. *Astrophys. J.* **303**, 39 (1986).
87. A. Ferrara, E. Tolstoy. The role of stellar feedback and dark matter in the evolution of dwarf galaxies. *Mon. Not. R. Astron. Soc.* **313**, 291 (2000).
88. J.I. Read, G. Gilmore. Mass loss from dwarf spheroidal galaxies: The origins of shallow dark matter cores and exponential surface brightness profiles. *Mon. Not. R. Astron. Soc.* **356**, 107 (2005).
89. J.I. Read, A.P. Pontzen, M. Viel. On the formation of dwarf galaxies and stellar haloes. *Mon. Not. R. Astron. Soc.* **371**, 885 (2006).
90. S. Mashchenko, J. Wadsley, H.M.P. Couchman. Stellar feedback in dwarf galaxy formation. *Science* **319**, 174 (2008).
91. A. Pontzen, F. Governato. How supernova feedback turns dark matter cusps into cores. *Mon. Not. R. Astron. Soc.* **421**, 3464 (2012).
92. F. Governato, A. Zolotov, A. Pontzen, C. Christensen, S.H. Oh, A.M. Brooks, T. Quinn, S. Shen, J. Wadsley. Cuspy no more: how outflows affect the central dark matter and baryon distribution in cold dark matter galaxies. *Mon. Not. R. Astron. Soc.* **422**, 1231 (2012).
93. R. Teyssier, A. Pontzen, Y. Dubois, J.I. Read. Cuspcore transformations in dwarf galaxies: Observational predictions. *Mon. Not. R. Astron. Soc.* **429**, 3068 (2013).
94. A. Di Cintio, C.B. Brook, A.V. Macciò, G.S. Stinson, A. Knebe, A. A. Dutton, J. Wadsley. The dependence of dark matter profiles on the stellar-to-halo mass ratio: A prediction for cusps versus cores *Mon. Not. R. Astron. Soc.* **437**, 415 (2014).

95. J.I. Read, O. Agertz, M.L.M. Collins. Dark matter cores all the way down. *Mon. Not. R. Astron. Soc.* **459**, 2573 (2016).

Received 12.06.18

*А.В. Рудаковський, Д.О. Савченко*

НОВА МОДЕЛЬ ПРОСТОРОВОГО РОЗПОДІЛУ ГУСТИНИ В ГАЛО ФЕРМІОННОЇ ТЕМНОЇ МАТЕРІЇ

Р е з ю м е

В цій роботі ми пропонуємо нову модель розподілу густини в гало, утвореного з теплої темної матерії. Ця модель описується одним параметром мікрофізики – масою частинки темної матерії (чи, що еквівалентно, максимальним значенням фазової густини). Знаючи масу частинки темної матерії та параметри, що описують розподіл густини на периферії гало, наша модель описує поведінку густини у внутрішніх областях гало. Для випадку початкового розподілу Фермі–Дірака, ми успішно відтворили результати симуляцій [28, 29]. Також, нами були розраховані радіуси центральних областей для гало карликових сферичних галактик утворених з теплої темної матерії з масами частинок $m_{\rm FD} = 100$, 200, 300, 400 еВ.